J Mater Sci (2015) 50:6748–6756
DOI 10.1007/s10853-015-9230-7

Reduction of electromigration damage in SAC305 solder joints by adding Ni nanoparticles through flux doping

M. Nasir Bashir[1] · A. S. M. A. Haseeb[1] · Abu Zayed Mohammad Saliqur Rahman[1] · M. A. Fazal[1] · C. R. Kao[2]

Received: 20 April 2015 / Accepted: 1 July 2015 / Published online: 11 July 2015
© Springer Science+Business Media New York 2015

Abstract The characteristics of interfacial intermetallic compounds (IMCs) can have serious impact on the reliability of solder joints. In this study, Ni nanoparticles (NPs) were added to SAC305 solder/Cu substrate interface by flux mixing. The effects of Ni NP addition on electromigration (EM) under high current density were investigated. EM tests with a maximum duration of 1128 h were conducted under a current density of 1×10^4 A/cm^2, at 80 ± 3 °C on the solders prepared using 0 and 2 wt% Ni NPs-doped flux. At 2 wt% Ni NPs addition to flux, the growth rate of interfacial IMC at the anode side decreased by more than five times. No significant change in electrical resistance was observed in 2 wt% samples for up to 1128 h. Ni NP addition at the solder/substrate through flux mixing is, therefore, expected to lead to more reliable solder joints.

Introduction

A recent focus in electronic manufacturing is to achieve high-performance electronic devices with much smaller size and slimmer form factor. Because of the miniaturization of microelectronic devices, the size of solder joint is being down-scaled and the operating current density in the package increased [1, 2]. Electromigration (EM) has therefore become one of the main reliability issues in microelectronic packaging [1, 3, 4]. During EM, atoms move along the direction of electron flow towards the anode side of the solder joint. As a result, voids, cracks, or damages can be generated at the cathode side [5–7]. High current density in small solder joints increases the occurrence of EM failures [8]. Researchers are putting a great deal of efforts to improve the reliability of lead-free solders in EM by minor addition(s), either in the form of alloying element(s) [9, 10] or as micro/nano particles [11–13]. Reported studies on the particle addition mainly use paste mixing [1, 14, 15] methods. In these cases, the particles are mixed throughout the solder matrix. Alloying additions through metallurgical routes also mix the element throughout the bulk solder. Recently, we have developed a flux mixing technique [16] which allows the addition of nanoparticles (NPs) mainly at the solder/substrate interface. The process essentially involves the application of Ni NP-doped commercial flux at the solder substrate interface prior to the reflow. The characteristics of the intermetallic (IMC) layers at the solder/substrate interfaces play an important role in determining the reliability of the solder joints. This is particularly important in small solder joints, where the interfacial IMCs constitute a large volume fraction of the joints. The flux mixing technique of NP addition allows us to study the effects of the modification of the interface caused by NP on the EM behavior of solder joints.

It may be noted that a partial dissolution of under bump metallization (UBM) during reflow e.g., the Ni layer can also supply Ni atoms to the solder. However, the choice of materials for UBM is limited by processing techniques

✉ A. S. M. A. Haseeb
haseeb@um.edu.my

✉ Abu Zayed Mohammad Saliqur Rahman
zayed@um.edu.my

M. Nasir Bashir
m.nsr8080@yahoo.com

[1] Department of Mechanical Engineering, University of Malaya, 50603 Kuala Lumpur, Malaysia

[2] Department of Materials Science and Engineering, National Taiwan University, Taipei 106, Taiwan

such as electroplating or vapor deposition. NP addition can allow a wide choice of elements to be added without additional processing steps. It has been demonstrated that elements like Cu [17], Ni [14], Co [18], and Zn [19] etc., can be incorporated into solder through NPs addition.

In this work, we report on the effects of nickel (Ni) NPs addition at the interface between Sn–3 %Ag–0.5 %Cu (SAC305) solder and copper substrate. The solder joints were prepared by the flux mixing method. The resulting solder joints were investigated for their interfacial characteristics and EM behavior. Results show that the addition of Ni NPs through flux doping modifies the morphology of interfacial IMCs, minimizes the polarity effect induced by EM, and suppresses the crack and void formation in SAC305 lead-free solder joints. To the best of our knowledge, this is the first time that the effects of the Ni NP addition at the solder/substrate interface on the EM behavior have been reported.

Experimental

Two types of lead-free solder joints were prepared using SAC305 solder balls (DUKSAN HI-METAL CO., LTD) and a commercial water soluble flux (Sparkle Flux WF-6317, Japan). For one group of samples, as-received flux was used without any NP addition. This group of sample is designated as SAC305 + 0 wt% Ni NPs. The second group of samples was prepared using a flux doped with 2 wt% Ni NPs. The latter sample is designated as SAC305 + 2 wt% Ni NPs. Nickel NPs (Accumet Materials, Co., USA) used in this study have an average diameter of 44 nm. Based on our previous studies [14, 15, 17], a part of the NPs is expected to enter the solder joints. Since it is difficult to measure the exact amount of NPs that enter the joint, we use the nominal amount of 2 wt% for sample designation purposes. Ni NPs were mixed with the flux mechanically for 30 min. Two pure copper wires with a diameter of 0.5 mm and a length of 12 mm were polished from the end. After polishing, the Cu wires were cleaned with 10 % sulphuric acid and distilled water. Polished side of copper wires was dipped into the as-received or NP-doped flux depending upon the type of sample prepared. A solder ball SAC305 with a diameter of 0.5 mm was dipped into the as-received or NP-doped flux. A pair of Cu wires and a solder ball was then placed in an aluminum die. The solder ball was placed between the polished ends of both Cu wires and their positions were adjusted on the die under a microscope. A line-type Cu/solder/Cu sample was assembled on the die as illustrated in Fig. 1a. The entire assembly was placed in a reflow oven and reflowed at 245 °C for 45 s. After the reflow, the line-type Cu/solder/Cu joint sample was taken out from the aluminum die. The sample was then mounted in epoxy resin and ground. The dimensions of solder joint are shown in Fig. 1. The cross section of the solder joint was calculated as 0.05 mm^2 by using the following equation:

$$\text{Cross-sectional area} = \frac{R^2}{2}\left(\frac{\pi}{180}C - \sin C\right), \quad (1)$$

where R is the radius of the wire and C is central angle in degrees.

The prepared sample was placed in a furnace and connected with a DC power supply (Leybold Didactic GMBH 521 55). EM test was operated at a constant current density of 1×10^4 A/cm^2 at 80 ± 3 °C. Operating temperature was set below the melting temperature of epoxy (130 °C). Epoxy resin was used to hold and protect the sample during grinding, polishing, and EM test running. The experiment was operated under normal atmosphere using an oven (Memmert Company Beschickung-loading model 100-800). A thermocouple was used to measure the temperature during EM test. The tip of thermocouple was placed on the solder joint during the measurement. EM tests were conducted for four different durations, such as 192, 384, 768, and 1128 h. After conducting EM test for specific periods of time, the samples were polished in order to investigate IMCs morphology by scanning electron microscope (SEM), field emission scanning electron microscope (FESEM), and energy-dispersive X-ray spectroscope (EDX) analysis. Image analysis software (Olympus SZX10) was used to measure area covered by the interfacial IMCs on the cross section. The average thickness of the IMCs was then calculated by dividing the IMCs area by length. Resistance was measured using digital data acquisition computerized device (Agilent 34972A) under a microscope. All the resistance measurements were repeated at least seven times on three different days and the average is reported.

Results

Figure 2a and b shows the SEM micrographs of as-reflowed samples of SAC305 solder joints. Micrographs of the interfaces at both ends of the joint are shown for each sample. In the case of SAC305 sample, the typical scallop type Cu_6Sn_5 IMC layer is visible at both interfaces. At high magnification the occurrence of a thin layer of Cu_3Sn was observed in an earlier work as well [20]. In the vicinity of interface, eutectic structure of fine Ag_3Sn/Cu_6Sn_5 is observed. The average thickness of IMCs at the interfaces is 3.0 µm.

Figure 2c and d shows the interfacial microstructures at both ends of the SAC305 + 2 wt% Ni NPs solder joints. Upon adding Ni NPs to the flux, we found a significant

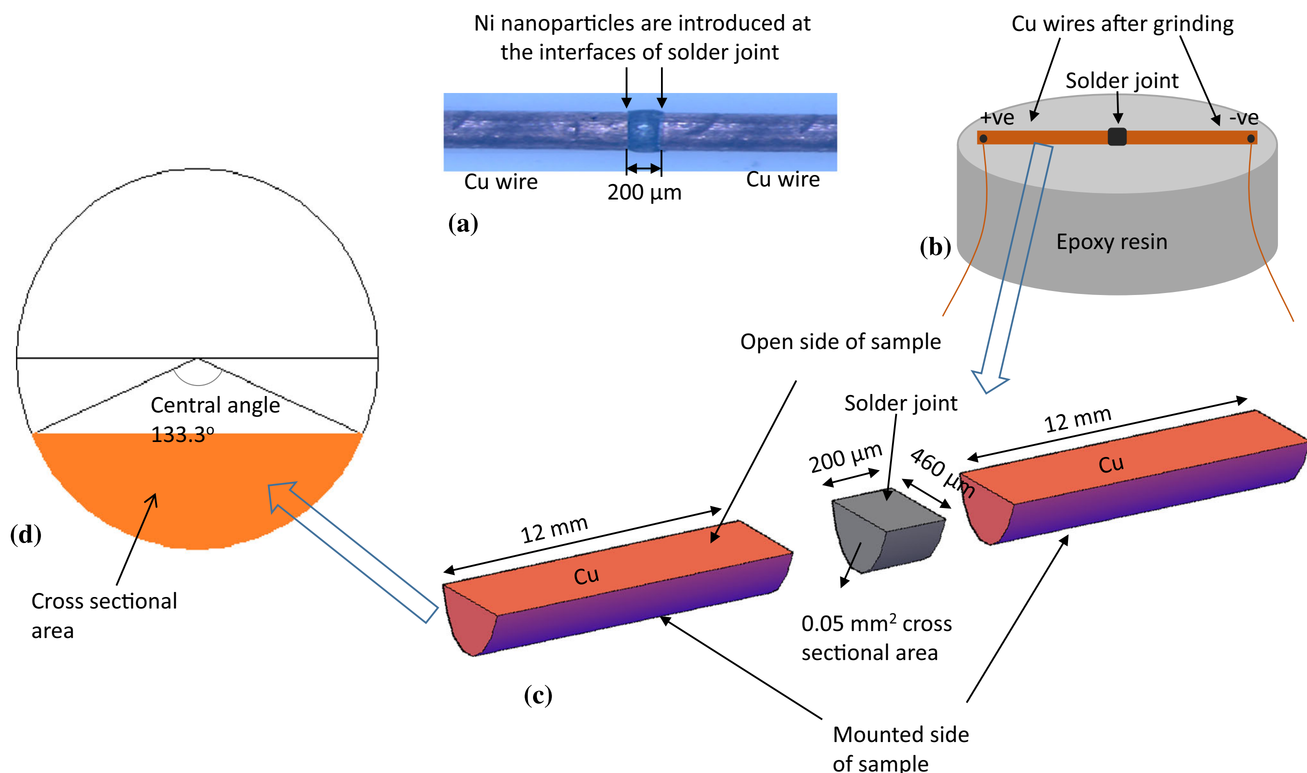

Fig. 1 **a** Photograph of a prepared line type Cu/solder/Cu solder joint, **b** mounted and ground sample in epoxy resin used for electromigration, **c** schematic diagram of the sample with all dimensions and, **d** description of central angle used for measurement of cross-sectional area

Fig. 2 SEM backscattered electron images of **a**, **b** SAC305 and **c**, **d** SAC305 + 2 wt% Ni NPs solder joints. Each micrograph corresponds to one end of the joint

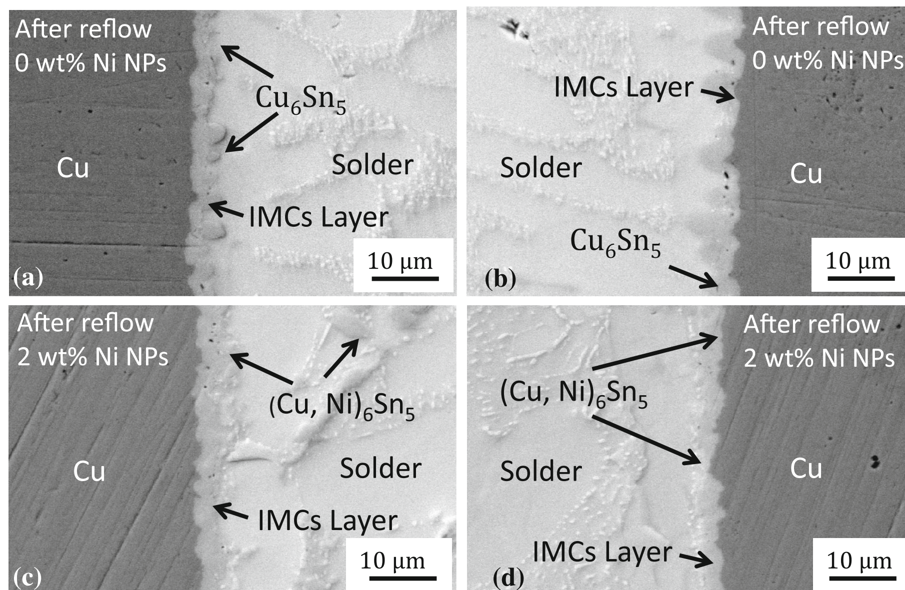

impact of Ni NPs on the interfacial microstructure of the solder joint. The morphology of the Cu_6Sn_5 IMC layer has changed from scallop type to a more planar type. The average thickness of the IMC layers becomes 3.9 µm which is somewhat higher than that for the SAC305 sample. EDX analysis was performed on different IMC phases in the SAC305 + 2 wt% Ni NPs sample. The average elemental composition of the phases is given in Table 1. It is seen in the table that the interfacial IMC contains Ni. The distribution of Ni in the interfacial IMC is not so uniform. The Ni content is 2.26 wt% at the solder side while it is lower at the substrate side (0.96 wt%). Similar observation

Table 1 EDX elemental compositions of IMC phases in SAC305 + 2 wt% Ni NP sample

Location	Element composition (wt%)			
	Cu	Ag	Sn	Ni
Interfacial IMC layer near to solder	53.99	0.39	43.37	2.26
Interfacial IMCs near to Cu substrate	54.01	0.23	44.76	0.96
IMCs in solder matrix	51.21	0.19	46.61	1.86

was made in an earlier work [14]. Some larger particles with a darker contrast are also seen in the matrix near the interfacial IMC. EDX analysis identified them as $(Cu, Ni)_6Sn_5$ particles. The IMC particles in the solder matrix near the interface contain an average of 1.86 wt%.

Figure 3 shows the effect of EM on the SAC305 solder joint after different time intervals. Figure 3a, b, c, and d shows the cross-sectional microstructures at cathode side after 192, 384, 768, and 1128 h, respectively; while Fig. 3e, f, g, and h shows that at the anode side after 192, 384, 768 and, 1128 h, respectively. At the cathode side, the thickness of the interfacial IMCs has decreased from 3.0 to 2.5, 1.7, 1.6, and 1.3 µm after the EM test at increasing time intervals. After 1128 h of EM, cracks and voids appear at the cathode side. On the other hand, the IMC thickness has increased from 3.0 to 3.8, 4.8, 7.9, and 9.5 µm at anode side with the current stressing time. No crack or damage is found at the anode side.

Figure 4a, b, c, and d shows the cross-sectional microstructures of interfacial IMCs at the cathode side of SAC305 + 2 wt% Ni NPs samples subjected to EM tests for 192, 384, 768 and 1128 h respectively. The microstructures of the IMCs at the anode side are shown in Fig. 4e, f, g and h tested for EM time of 192, 384, 768 and 1128 h respectively. At the cathode side, no systematic change in the thickness or morphology of the interfacial IMC layer is observed. The average values of IMC thickness at cathode and anode side of both solder joint are given in Table 2. At 1128 h, cracks appear near the interface at the cathode side. However, the extent of crack and damage after 1128 h of EM test is significantly less in SAC305 + 2 wt% Ni NPs as compared with that in the SAC305 sample (Fig. 4d and 3d). The thickness of interfacial IMC at the anode side increased from 3.9 µm to 4.1, 4.4, 4.5 and 4.8 µm with increasing EM time. However, as compared with SAC305, the increase in the interfacial IMC thickness at the anode side is much less in the SAC305 + 2 wt% Ni NPs sample.

The growth rate of IMCs at the anode side, namely Cu_6Sn_5 and $(Cu, Ni)_6Sn_5$ in solder joints was estimated from Figs. 3 and 4 (Table 3). The average anodic growth rate for Cu_6Sn_5 and $(Cu, Ni)_6Sn_5$ was found to be 1.46×10^{-6} and 2.72×10^{-7} µm/s, respectively.

Figure 5 shows the variation of thickness of the interfacial IMC at both cathode and anode sides of SAC305 and SAC305 + 2 wt% Ni NPs samples as a function of EM test time. The figure reveals that the interfacial IMC thickness in the SAC 305 sample markedly decreases and increases at the cathode and anode sides, respectively. On the other hand, no significant change in the IMC thickness was observed in the SAC305 + 2 wt% Ni NPs sample. It can therefore be concluded that the addition of Ni NPs at the interface makes the interfacial IMC much more stable during EM.

Figure 6 shows EDX elemental maps for different elements for SAC305 + 2 wt% Ni NPs subjected to 1128 h of EM test. SEM micrograph in Fig. 6a shows a contamination/artifact (round in shape), but it does not interfere with the main observations. Contamination occurred from the use of carbon tape during FESEM analysis to avoid the charging effects. Elemental map of Ni (Fig. 6d) shows that it is mainly concentrated at the interface. But a close observation of the Ni map reveals that Ni is also present in the solder matrix, particularly near to the interfaces which can be seen at the left and right side of Fig. 6d.

Figure 7 shows the electrical resistance of the soldered wire as a function of EM time for 0 and 2 wt% Ni-doped samples. The resistance increased with EM time in 0 wt% samples, whereas no significant change was observed for 2 wt% Ni samples.

Discussion

In this study, we focused on the effects of the addition of Ni NPs to SAC305 solder joints by flux mixing. A commercial water soluble flux mixed with 2 wt% Ni NPs was used for solder preparation. The resulting effects on the morphology and thickness of interfacial IMCs, and the EM performance of the solder joints have been investigated. It is seen that the addition of Ni NPs to the flux has a decisive influence on the as-reflowed morphology and thickness of interfacial IMC. Ni NPs addition has changed the usual scallop type morphology of Cu_6Sn_5 into a planer type. Ni NPs particles also increased the thickness of the interfacial IMC. EDX analysis confirmed the presence of Ni in the interfacial IMC leading to the formation of $(Cu, Ni)_6 Sn_5$ which can be expressed by following equation:

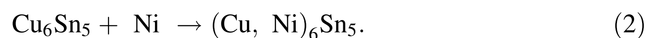

$$Cu_6Sn_5 + Ni \rightarrow (Cu, Ni)_6Sn_5. \quad (2)$$

Ni was also detected in the Cu_6Sn_5 IMC particles in the matrix near the interface. These results are similar to the case when Ni is added to SAC solder as a metallurgical alloy addition [9]. Very similar results were also found when Ni NPs were added to SAC solder paste and was subjected to reflow [15]. It was concluded in the earlier

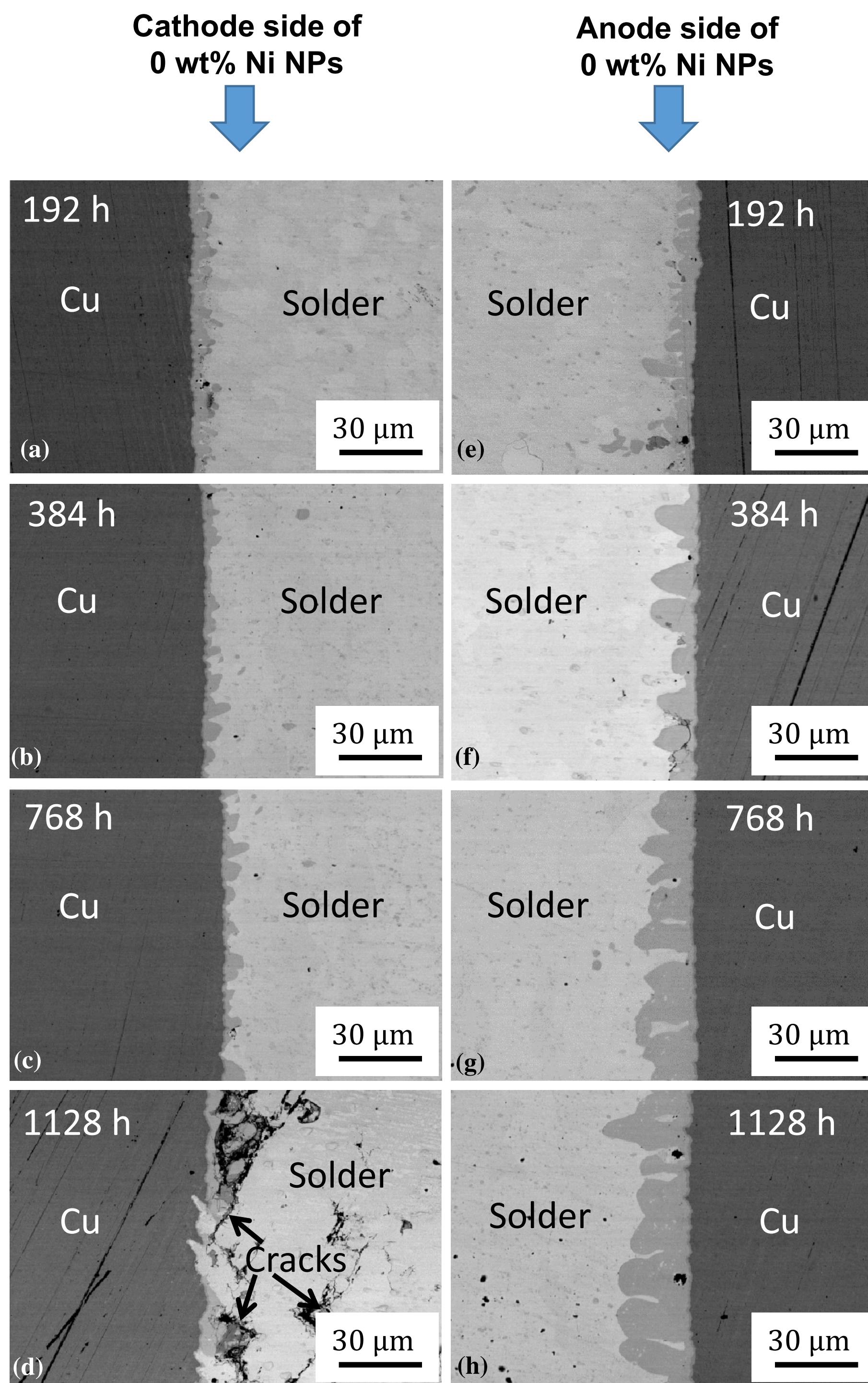

Fig. 3 FESEM backscattered electron images of SAC305 solder joint after EM test for 192, 384, 768, and 1128 h. **a–d** show cathode side, while **e–h** show anode side

study that Ni NPs, when mixed with solder paste, undergo in situ alloying during reflow through reactive dissolution. Similar observations were made for Co and Zn NPs as well [18, 21, 22]. It is, therefore, suggested that when a Ni NP-doped flux is applied to the solder ball/substrate interface, Ni NPs undergo reactive dissolution and is incorporated into the solder joint through in situ alloying. It was reported earlier that when Ni NPs were added to solder paste, less than one-third of nickel entered the solder joint after reflow. The rest was discarded to the flux residue. In the present case, Ni NPs are added to the flux at 2 wt%. It is highly likely that only a fraction of it entered the solder. It is difficult to find out exactly how much of Ni NPs is retained in the solder. However, it is clear that doping of

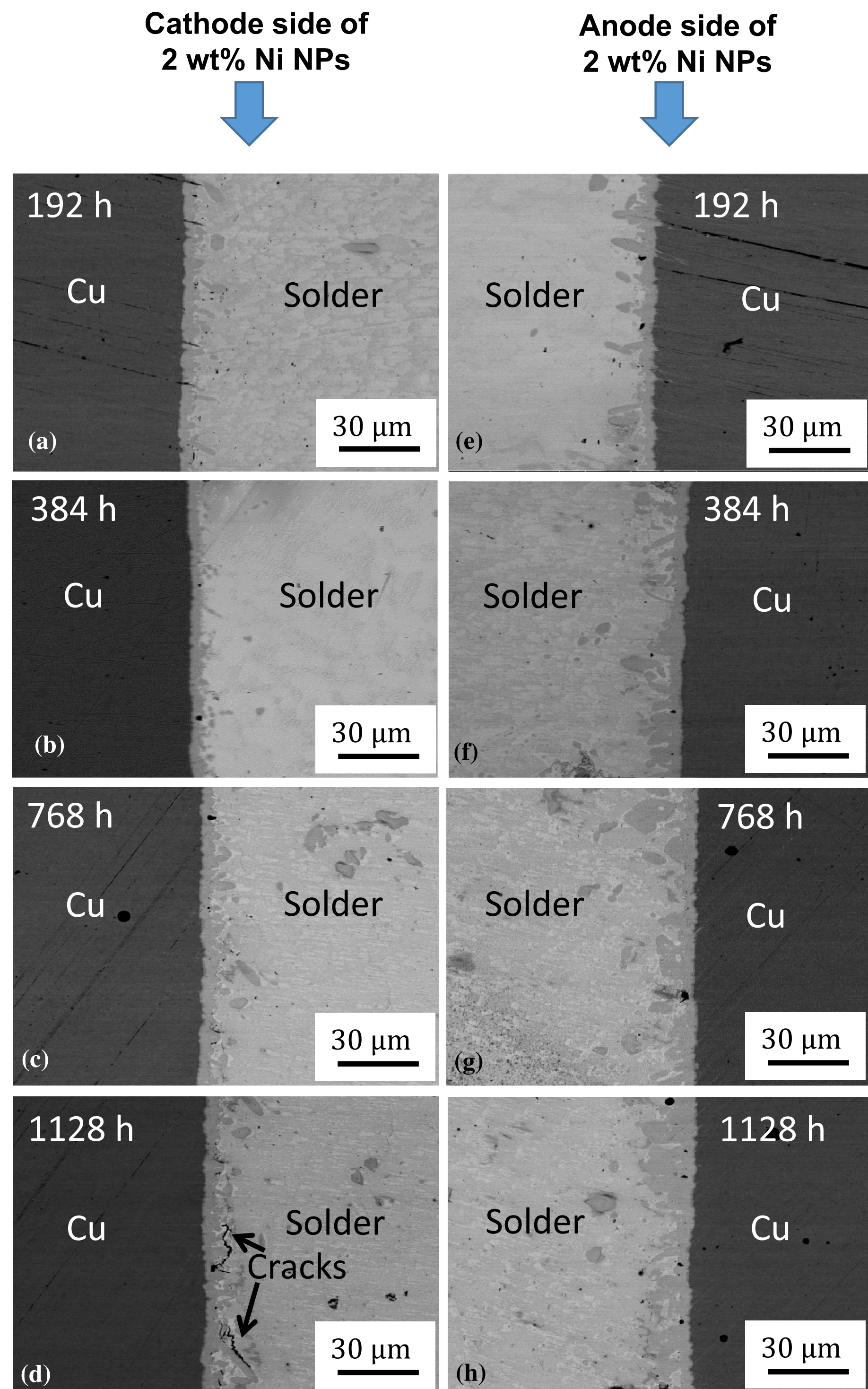

Fig. 4 FESEM backscattered electron images of SAC305 + 2 wt% Ni NPs solder joint after EM test for 192, 384, 768 and 1128 h. **a–d** show cathode side, while **e–h** show anode side

the flux with 2 wt% Ni NPs resulted in the incorporation of enough Ni in the solder so as to have a distinct influence. Ni NP addition is also seen to influence the EM characteristics of the solder joint which is suggested to be related to the alloying effect. With a high current density (order of 1×10^4 A/cm^2), EM usually influences the migration of Cu atoms from substrate to solder joint. This leads to reliability concern for the solder joint. Rapid growth of the interfacial IMCs at anode side could be well controlled by managing the diffusion of Cu atoms from the substrate. Other than current density, diffusion of Cu atoms also depends on temperature and duration of EM. Therefore, we

Table 2 The average values of IMC thickness at cathode and anode side of SAC305 and SAC305 + 2 wt% NPs-doped flux solder joint

	Time (h)	IMC thickness of 0 wt% sample (μm)	IMC thickness of 2 wt% sample (μm)
Cathode	0	3.0	3.9
	192	2.5	3.7
	384	1.7	3.5
	768	1.6	3.5
	1128	1.3	3.4
Anode	0	3.0	3.9
	192	3.8	4.1
	384	4.8	4.4
	768	7.9	4.5
	1128	9.5	4.8

Table 3 Anodic growth rate of IMCs in SAC305 solder with 0 and 2 wt% Ni-doped flux at various electromigration time interval

EM time (h)	Cu_6Sn_5 ($\times 10^{-6}$ μm/s)	$(Cu, Ni)_6Sn_5$ ($\times 10^{-7}$ μm/s)
192	1.157	2.893
384	1.302	3.616
768	1.772	2.170
1128	1.600	2.216
Average	1.46 ± 0.28	2.72 ± 0.68

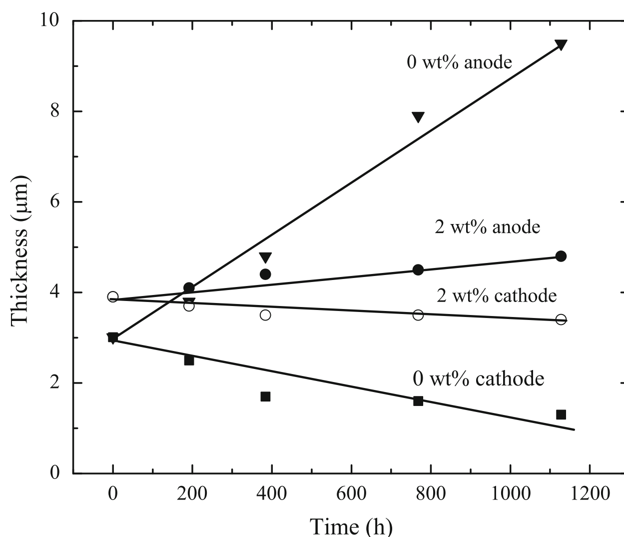

Fig. 5 IMC thickness variation as a function of electromigration time in cathode and anode of SAC305 solder with 0 and 2 wt% Ni-doped flux

increased the duration of EM test to see the further effect on Cu diffusion. In SAC 305 solder joint, a substantial increase of IMC thickness at the anode side was observed in Fig. 3a–h with a corresponding decrease at cathode side

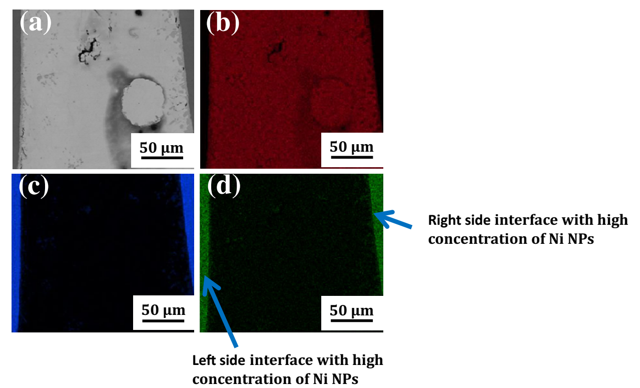

Fig. 6 EDX elemental maps of SAC305 + 2 wt% Ni NPs solder joint after EM test for 1128 h. **a** SEM Image, elemental maps for **b** Sn, **c** Cu, and **d** Ni

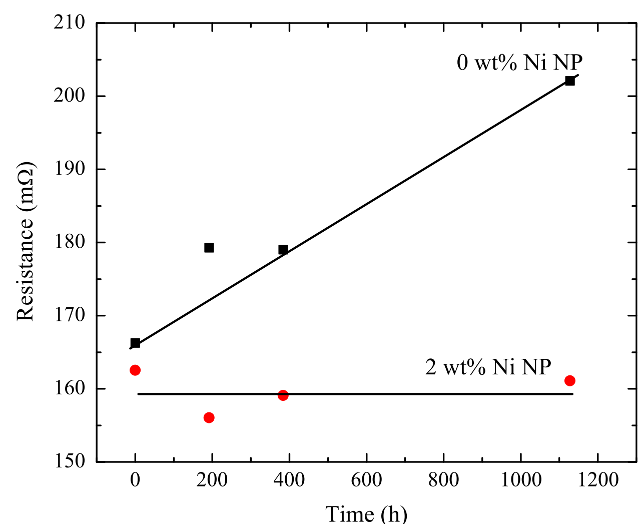

Fig. 7 Resistance of SAC305 solder with 0 and 2 wt% Ni-doped flux as a function of electromigration time

as the duration of EM test increased as described in the Table 2. High current density causes heavy electron wind flow through the sample. Cu atoms start to migrate in the direction of electron flow from cathode toward the anode side because of drifting and collision with the electrons. Gradually, Cu atoms begin to form a thicker layer of IMCs such as Cu_6Sn_5 at anode side by reacting with Sn atoms [23]. If IMCs become thicker, it could reduce the mechanical reliability of solder joint because of the brittleness of the IMC [24]. On the other hand, directional migration of Cu atoms toward the anode side creates vacancy, cracks, and voids at the cathode side [9]. Serrated cathode dissolution phenomenon [24] can be seen in Fig. 3d. The addition of a small quantity of Ni NPs slowed down the dissolution process at the cathode (Fig. 4d). Figure 8 shows the schematic diagram representing microstructure changes at interfaces of SAC305 and

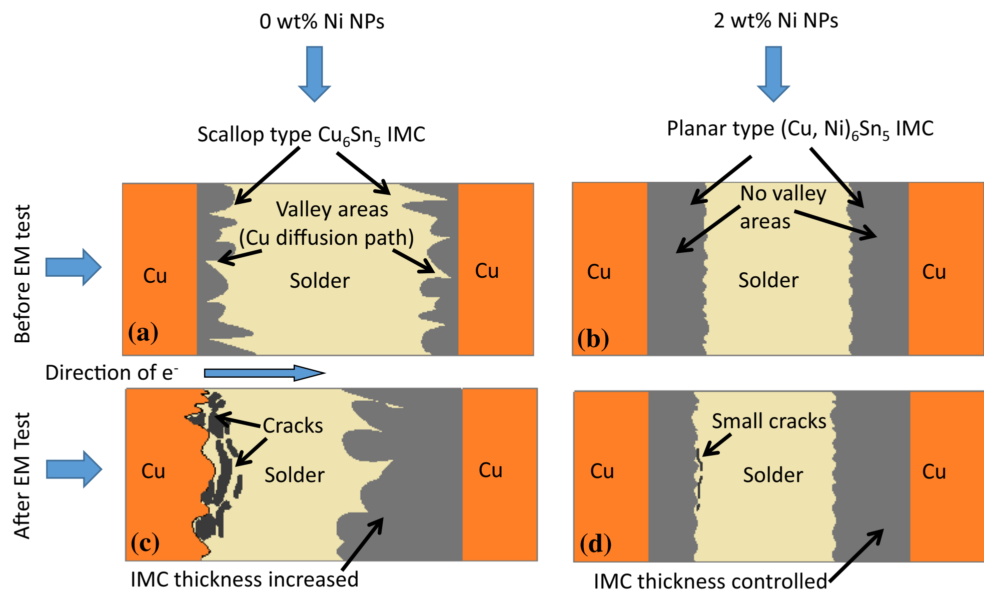

Fig. 8 Schematic diagrams presenting microstructure changes in SAC305 and SAC305 + 2 wt% Ni NPs solder joints **a**, **b** before while **c**, **d** after EM test

SAC305 + 2 wt% Ni NPs solder joints before and after EM.

Polarity effect of EM is also one of the challenging factors causing solder joint failure. During EM, Cu atoms are accumulated at anode but depleted at the cathode which results in more vacancies at the cathode side than at the anode side as proposed in the Nabarro-Herring model. Figure 4 shows that in the SAC305 + 2 wt% Ni NPs solder joint, polarity effect was suppressed significantly. It also reduced Cu diffusion into the solder joint and resisted rapid growth of interfacial IMCs at cathode and anode side as described in result section. Similarly, Ran et al. found the suppression of polarity effect by addition of Ni and Co in SAC solder joint [9, 25]. After the migration of Cu atoms, the created vacancies at cathode side produce disconnection at interfaces. This disconnection reduces the conductivity of current and increases the resistance in the solder joint [26]. In this case, heavy electron wind changes its conducting path and tries to flow from the connected area of the joint. Usually, current prefers to conduct from well conducting and connected area of the joint. So in this case, most of the electron wind leaves the disconnected area of joint and attacks at connected area which creates a non-uniform current distribution and increases the current density at that area. Due to the increment in current density at that particular area, Cu atoms get more energy to leave their position and increase the Cu diffusion rate, produce more void and cracks at cathode side [7, 27, 28], increase the rapid growth of IMC at anode side [29], and finally lead to failure and separate the solder joint from substrate at cathode interfaces. It is observed that Ni NPs can control the crack which leads to better resistance stability as compared to pure SAC305 samples. From all the experiments, positive effect of Ni addition on solder joints is found.

Ni atoms can be easily incorporated into the interface and matrix of solder joint during reflow process by the reactive desolation of Ni NPs of their high surface to volume ratio and high reactivity [14, 30]. Crystal structure of Ni atoms is cubic as similar to crystal structure of Cu atoms. Therefore, Ni atoms substitute Cu atoms in Cu_6Sn_5 and create $(Cu, Ni)_6$ Sn_5 at the interfaces and in the solder bulk [31]. Gao et al. have shown, based on thermodynamic calculation, that $(Cu, Ni)_6$ Sn_5 is more stable than Cu_6Sn_5 [32]. Yu et al. have also obtained the similar results [33]. It was also verified by FESEM and EDX analysis elsewhere [34]. Thus the formation of $(Cu, Ni)_6$ Sn_5 will reduce the dissolution of Cu and will retard the flux of Cu atoms from the interfaces at the cathode to anode side.

Moreover, the conversion of scallop-to-planer type IMCs at interface of Ni NPs-doped SAC305 solder joint takes place. Cu atoms usually diffuse from valley area between the two neighboring scallops [9, 25]. Thickness at valley area is much lower than average thickness at planer type IMCs. Therefore, planar type IMCs can act as diffusion barrier for Cu atoms. The addition of Ni NPs through flux mixing thus seems to improve the EM performance of solder joints.

Conclusions

SAC305 and SAC + 2 wt% Ni (NPs) solder joints were investigated at 80 ± 3 °C with 10^4 A/cm^2 for different time intervals. By adding 2 wt% Ni NPs to the flux, thickness of IMCs at cathode and anode side can be controlled during EM test. Ni NPs suppress the polarity effect; reduce the cracks, voids, and damages in SAC305 solder

joint. It decreased the average anodic growth rate of IMC from 1.46×10^{-6} μm to 2.72×10^{-7} μm/s. Resistance also shows better stability than SAC305 sample. It could be reasonably concluded that the addition of 2 wt% Ni NPs-doped flux reduces EM damages, which is expected to lead to longer lifespan of SAC305 solder joint.

Acknowledgements The authors acknowledge the financial support of High Impact Research grant (UM.C/HIR/MOHE/ENG/26, Grant No. D000026-16001).

References

1. Ma L, Xu G, Sun J, Guo F, Wang X (2011) Effects of Co additions on electromigration behaviors in Sn–3.0Ag–0.5Cu-based solder joint. J Mater Sci 50:4896–4905
2. Huang ML, Zhou Q, Zhao N, Liu XY, Zhang ZJ (2014) Reverse polarity effect and cross-solder interaction in Cu/Sn–9Zn/Ni interconnect during liquid–solid electromigration. J Mater Sci 49:1755–1763
3. Lin YH, Tsai CM, Hu YC, Lin YL, Kao CR (2005) Electromigration-induced failure in flip-chip solder joints. J Electron Mater 34:27–33
4. Chen C, Liang SW (2007) Electromigration issues in lead-free solder joints. In: Subramanaian KN (ed) Lead-free electronic solders. Springer, New York, pp 259–268
5. Xu L, Pang JHL, Ren F, Tu KN (2006) Electromigration effect on intermetallic growth and Young's modulus in SAC solder joint. J Electron Mater 35:2116–2125
6. Chen LD, Huang ML, Zhou SM (2010) Effect of electromigration on intermetallic compound formation in line-type Cu/Sn/Cu interconnect. J Alloy Compd 504:535–541
7. Cm Hsu, Sw Chen (2013) Interfacial reactions with and without current stressing at Sn–Co/Ag and Sn–Co/Cu solder joints. J Mater Sci 48:6640–6646
8. Zuo Y, Ma L, Liu S, Wang T, Guo F, Wang X (2013) The coupling effects of thermal cycling and high current density on Sn58Bi solder joints. J Mater Sci 48:2318–2325
9. Zhao R, Ma L, Liu YZS, Guo F (2013) Retarding electromigration in lead-free solder joints by alloying and composite approaches. J Electron Mater 42:280–287
10. Wang YW, Chang CC, Kao CR (2009) Minimum effective Ni addition to SnAgCu solders for retarding Cu_3Sn growth. J Alloy Compd 478:L1–L4
11. Zhang R, Xu G, Wang X, Guo F, Lee A, Subramanian KN (2010) Electromigration in Sn–Bi modified with polyhedral oligomeric silsesquioxane. J Electron Mater 39:2513–2521
12. Rhee H, Guo F, Lee JG, Chen KC, Subramanian KN (2003) Effects of intermetallic morphology at the metallic particle/solder interface on mechanical properties of Sn–Ag-based solder joints. J Electron Mater 32:1257–1264
13. Fuo F, Xu G, Ge H (2009) Electromigration behaviors in Sb particle-reinforced composite eutectic SnAgCu solder joints. J Mater Sci 44:5595–5601
14. Tay SL, Haseeb ASMA, Johan MR, Munroe PR, Quadir MZ (2013) Influence of Ni nanoparticle on the morphology and growth of interfacial intermetallic compounds between Sn–3.8Ag–0.7Cu lead-free solder and copper substrate. Intermetallics 33:8–15
15. Tay SL, Haseeb ASMA, Johan MR (2011) Addition of cobalt nanoparticles into Sn–3.8Ag–0.7Cu lead-free solder by paste mixing. Solder Surf Mt Tech 23:10–14
16. Sujan GK, Haseeb ASMA, Afifi ABM (2014) Effects of metallic nanoparticle doped flux on the interfacial intermetallic compounds between lead-free solder ball and copper substrate. Mater Charact 97:199–209
17. Nadia A, Haseeb ASMA (2012) Effects of addition of copper particles of different size to Sn–3.5Ag solder. J Mater Sci 23:86–93
18. Haseeb ASMA, Leng TS (2011) Effects of Co nanoparticle addition to Sn–3.8 Ag–0.7 Cu solder on interfacial structure after reflow and ageing. Intermetallics 19:707–712
19. Haseeb ASMA, Leong YM, Arafat MM (2014) In situ alloying of Sn–3.5Ag solder during reflow through Zn nanoparticle addition and its effects on interfacial intermetallic layers. Intermetallics 54:86–94
20. Rao CBSS, Weng J, Shen L, Lee TK, Zeng KY (2010) Morphology and mechanical properties of intermetallic compounds in SnAgCu solder joints. Microelectron Eng 87:2416–2422
21. Chan YH, Arafat MM, Haseeb ASMA (2013) Effects of reflow on the interfacial characteristics between Zn nanoparticles containing Sn–3.8Ag–0.7Cu solder and copper substrate. Solder Surf Mt Tech 25:91–98
22. Arafat MM, Haseeb ASMA, Johan MR (2011) Interfacial reaction and dissolution behavior of Cu substrate in molten Sn–3.8Ag–0.7Cu in the presence of Mo nanoparticles. Solder Surf Mt Tech 23:140–149
23. Gan H, Tu KN (2005) Polarity effect of electromigration on kinetics of intermetallic compound formation in Pb-free solder V-groove samples. J Appl Phys 97:063514
24. Ren F, Nah J, Xiong B, Luhua Xu, Pang JHL (2006) Electromigration induced ductile-to-brittle transition in lead-free solder joints. Appl Phys Lett 89:141914
25. Tu KN, Lee TY, Jang JW, Li L, Frear DR, Zeng K, Kivilahti JK (2001) Wetting reaction versus solid state aging of eutectic SnPb on Cu. J Appl Phys 89:4843–4849
26. Chang YW, Liang SW, Chen C (2006) Study of void formation due to electromigration in flip-chip solder joints using Kelvin bump probes. Appl Phys Lett 89:032103
27. Xie HX, Friedman D, Mirpuri K, Chawla N (2014) Electromigration damage characterization in Sn–3.9Ag–0.7Cu and Sn–3.9Ag–0.7Cu–0.5Ce solder joints by three-dimensional X-ray tomography and scanning electron microscopy. J Electron Mater 43:33–42
28. Sun J, Xu G, Gou F, Xia Z, Lei Y, Shi Y, Li X, Wang X (2011) Effects of electromigration on resistance changes in eutectic SnBi solder joints. J Mater Sci 46:3544–3549
29. He H, Xu G, Guo F (2010) Electromigration-enhanced intermetallic growth and phase evolution in Cu/Sn–58Bi/Cu solder joints. J Mater Sci 45:929
30. Liu PC, Hsieh JH, Li C, Chang YK, Yang CC (2009) Dissolution of Cu nanoparticles and antibacterial behaviors of TaN–Cu nanocomposite thin films. Thin Solid Films 517:4956–4960
31. Gao F, Qu J, Takemoto T (2010) Additive occupancy in the Cu6Sn5-based intermetallic compound between Sn–3.5Ag solder and Cu studied using a first-principles approach. J Electron Mater 39:426–432
32. Gao F, Takemoto T, Nishikawa H (2006) Effects of Co and Ni addition on reactive diffusion between Sn–3.5Ag solder and Cu during soldering and annealing. Mater Sci Eng, A 420:39–46
33. Yu C, Liu J, Lu H, Li P, Chen J (2007) First-principles investigation of the structural and electronic properties of $Cu_{6-x}Ni_XSn_5$ ($x = 0$, 1, 2) intermetallic compounds. Intermetallics 15:1471–1478
34. Rahman AZMS, Chia PY, Haseeb ASMA (2015) Mechanical properties of intermetallic compounds in electrodeposited multilayered thin film at small scale by nanoindentation. Mater Lett 147:50–53